Estimating the variability of contact parameter temperature dependence with the Monte Carlo Markov Chain method

Anni Määttänen, M. Douspis

GeoResJ 3-4 (2014) 46–55

Contents lists available at ScienceDirect

GeoResJ

journal homepage: www.elsevier.com/locate/GRJ

Estimating the variability of contact parameter temperature dependence with the Monte Carlo Markov Chain method

A. Määttänen [a,b,c,*], M. Douspis [d]

[a] Université Versailles St-Quentin, LATMOS-IPSL, 11 boulevard d'Alembert, 78280 Guyancourt, France
[b] Sorbonne Universités, UPMC Univ. Paris 06, LATMOS-IPSL, Guyancourt, France
[c] CNRS/INSU, LATMOS-IPSL, Guyancourt, France
[d] Institut d'Astrophysique Spatiale, CNRS (UMR8617) and Université Paris-Sud 11, Bâtiment 121, 91405 Orsay, France

ARTICLE INFO

Article history:
Received 2 April 2014
Revised 30 July 2014
Accepted 22 September 2014

Keywords:
Heterogeneous deposition mode ice nucleation
Laboratory experiment reanalysis
Contact parameter
Monte Carlo Markov Chains

ABSTRACT

Recent datasets on heterogeneous deposition mode ice nucleation have revealed a strong dependence of the contact parameter m on temperature, ranging from linear to exponential, depending on the experiments. We analyze recent datasets using a Monte Carlo Markov Chain method with the full classical nucleation theory including spherical and planar geometry. The method we use allows us to test models of the temperature dependence of the contact parameter and evaluate their performance. We estimate the applicability of different forms of contact parameter temperature dependence, including a new well-behaved suggestion. Such a function has a more physical behavior at high and low temperatures and might thus be more easily applicable in atmospheric modeling. However, because of their limited temperature range, the present datasets are unable to reveal the behavior of the contact parameter in low temperatures, and we are unable to fully validate the proposed function. We thus call for more heterogeneous nucleation experiments reaching low temperatures (<170 K). Such datasets may be significant for studies on, for example, polar mesospheric clouds, Mars ice clouds, and perhaps exoplanet clouds. This work provides a new framework, valid even for very small ice nucleus sizes, for analyzing heterogeneous nucleation datasets.

1. Introduction

The contact angle θ, or the wetting coefficient, is a crucial parameter in modeling heterogeneous nucleation. It describes the interaction between the forming cluster of molecules and the condensation/ice nucleus surface beneath. It depends on the nucleating vapor, and the properties of the forming cluster and the condensation/ice nucleus. However, it is not directly measurable, and it can not be easily derived from theory (Young's equation, [39]) without some empirical (measured) information on the parameters (surface tensions) it depends on. Strictly speaking, the theoretical contact angle and the one measured are not exactly equivalent, since the measured contact angle includes several effects related to the heterogeneity of the condensation/ice nucleus surface not accounted for in the theoretical definition. Often contact angles (or contact parameter $m = \cos\theta$, used hereafter, $m \in [-1, 1]$) and their dependence on other variables (temperature, mole fraction) are derived from experimental heterogeneous nucleation data. Through such experiments, the contact parameter is commonly derived from the observed critical saturation ratio at nucleation onset using classical nucleation theory, and the possible dependencies on other variables are deduced from repeated experiments in different conditions (see, e.g., [31]). This is normally the approach in the so-called single-α model (in our notation single-m), where the entire condensation nucleus population is characterized with a single value of the contact parameter m. This is also our approach in this paper. Other types of distributions for the contact parameter m have been used in the literature [37], such as the probability distribution function (PDF-α or PDF-m using our notation). Recent reviews can be found in Wheeler and Bertram [37] and Hoose and Möhler [11].

Ice crystal formation can happen through different pathways (deposition mode nucleation, contact freezing, immersion freezing, condensation freezing and homogeneous freezing, Pruppacher and Klett [27]). The heterogeneous processes (the first four of the list above) require the presence of ice nuclei (IN). Dust dominates the aerosol mass in the atmosphere of the Earth [29] and is a very good IN (e.g., [3,4]). Deposition mode ice nucleation on mineral

* Corresponding author at: Université Versailles St-Quentin, LATMOS-IPSL, 11 boulevard d'Alembert, 78280 Guyancourt, France.
E-mail address: anni.maattanen@latmos.ipsl.fr (A. Määttänen).

http://dx.doi.org/10.1016/j.grj.2014.09.002
2214-2428/

dust has been experimentally studied in different Continuous Flow Diffusion Chamber (CFDC) experiments by, for example, Welti et al. [36] and Koehler et al. [15], and in the AIDA (Aerosol Interactions and Dynamics in the Atmosphere) chamber by, for example, Möhler et al. [23], all of them anyhow focusing on terrestrial conditions. Numerous similar ice nucleation experiments have been made for terrestrial applications (see, e.g., [11] for a review).

On Mars mineral dust is ubiquitous in the atmosphere [13] and functions as the IN. Because of the absence of liquid phase in the prevailing low pressures and temperatures, heterogeneous deposition mode ice nucleation is the main nucleation mechanism in the Martian atmosphere for the two (separately) condensing substances, H_2O and CO_2 [19]. However, heterogeneous ice nucleation modeling for Mars suffers from lack of information on key nucleation parameters, such as the contact parameter. Until recently, only single values of contact parameter derived from different sources [38,9] without any temperature dependence were used for both H_2O and CO_2. Recently new datasets for heterogeneous deposition mode H_2O ice nucleation have been acquired by Iraci et al. [12] and Phebus et al. [26] who measured nucleation onset as a function of temperature in pure water vapor (with Martian vapor partial pressures) in a vacuum chamber. In addition, Ladino and Abbatt [16] and Cziczo et al. [2] recently published experimental results related to Martian water ice cloud formation using a CFDC and the AIDA chamber.

It can be noted that the experiment types for the determination of the contact parameter m are not always the same (vacuum chamber, CFDC, etc., see e.g., [31,16]). Combining datasets from different experimental setups might sometimes help increasing the temperature range or the number of data points, but there are caveats: the IN samples may not have been produced in the same way, and the available surface areas are not similar, causing differences in the nucleation ability of the particle samples. In addition, the analysis methods and the reported nucleation onset thresholds may be different. In general, the experiments have been conducted on samples of dust particles (for example, Arizona Test Dust, and others) and the contact parameter has been derived from the measured critical saturation ratios using the classical nucleation theory. A particularly elegant example is the paper by Chen et al. [1], who presented an analytical method based on the linearization of the nucleation theory to retrieve, from heterogeneous ice nucleation data, values related to the nucleation process and the IN properties. They also showed the importance of using spherical geometry if the IN were very small and noted that errors caused by the particle size on the retrieved contact parameter on dust may be particularly large compared to errors on other types of IN (soot, pollen, bacteria).

In this paper we present a new method for analyzing experimental heterogeneous ice nucleation data. For deriving the contact parameter we use the so-called Monte Carlo Markov Chain (hereafter MCMC) method to find the best fit to the data. In brief, we perform a data inversion: we find the best fit to the measured data simultaneously at all points for different functional forms of the temperature dependence of the contact angle ("m-models"). The method uses a full nucleation model to calculate the observables at each data point. This means all of the components of the nucleation rate equations are calculated at the conditions of the measurements instead of considering them (kinetic pre-factor, number of adsorbed monomers on the IN surface, etc.) constant as in some of the experimental articles.

For testing our method, we focus on certain recent experiments that are related to deposition mode ice nucleation (direct vapor-to-ice phase transition) of H_2O in a vacuum chamber. Iraci et al. [12] and Phebus et al. [26] showed a clear temperature dependence of the contact parameter of water on mineral dust, and they found that a linear trend described best this dependence in their data. Trainer et al. [31] showed by combining three datasets of water deposition nucleation on silicon and gold substrates, measured with the same experimental setup, that the best fit for the contact parameter m was acquired with an exponential dependence on temperature. The advantage of Trainer et al. [31] over Iraci et al. [12] and Phebus et al. [26] was their large temperature range: they saw the steep decrease of m below 200 K and the asymptotic behavior above 200 K, whereas the two other studies only saw the descending part of the m-curve just below 200 K. However, the caveat was that their substrates (silicon and gold) are not atmospherically relevant. We will study these three vacuum-chamber datasets with our MCMC technique.

2. Data

We use datasets of deposition mode ice nucleation in pure water vapor under Mars vapor partial pressure and temperature range [12,26,31]. Note that because the experiments used pure water vapor, in the following pressure means partial pressure of the vapor (and equals total pressure). Iraci et al. [12] and Phebus et al. [26] conducted their experiments on samples of dust particles (Arizona Test Dust [ATD], Smectite [SM], and Mars analog sample JSC-1 [JSC]), and Trainer et al. [31] reported measurements on gold and silicon substrates [Trainer]. In the experiments, the nucleation onset temperature was measured for different values of partial pressure. The subsets of data we have used for retrieving the contact parameter are plotted in Fig. 1. For each IN type, Iraci et al. [12] and Phebus et al. [26] published also the saturation ratio (S), calculated from the measured nucleation onset temperature, the partial pressure in the chamber, and the known saturation vapor pressure temperature dependence [24]. As these S-values are deduced from the measured nucleation onset temperature, we do not use them for the contact parameter determination. We test a posteriori, once the contact parameter has been determined from the measured temperature and vapor pressure values, if our deduced values of S are in agreement with those measured.

We have acquired the data used in Trainer et al [31] from Dr. M. G. Trainer (personal communication, 2011), on which we apply the same method. To carry out their study, Trainer et al. [31] combined their own dataset on water ice depositional nucleation on a silicon substrate with two other datasets [7,30]. Fortin et al. [7] studied the same vapor-substrate system (i.e., silicon), but Shilling et al. [30] used a gold substrate. Despite the two different substrates,

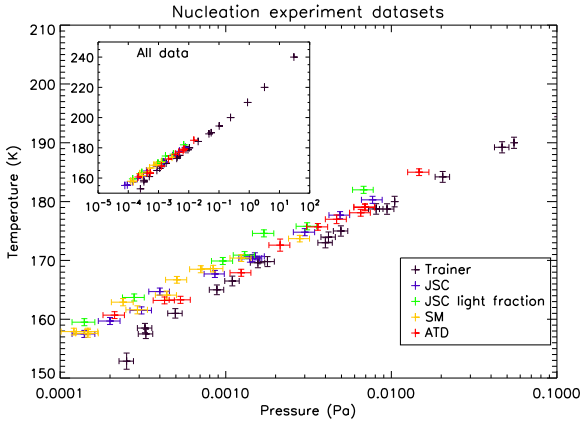

Fig. 1. Deposition mode ice nucleation onset temperature as a function of water vapor partial pressure (with error bars) for the three vacuum-chamber datasets [31,12,26]. The larger plot contains a zoom of the range T = [150–210 K] where most of the data points are found. The smaller plot on the left upper corner shows all data points. The abbreviations refer to the different datasets as explained in the text and in Table 1.

the idea of Trainer et al. [31] was to have a large range of temperatures covered by the full dataset to study the temperature dependence of m. This was done by combining the previous measurements with their new measurements going down to 150 K. The total temperature range was 150–240 K. We calculated some error bars that were not given in the dataset based on the error estimates given in the respective articles [7,30]. If a certain range was given for the relative error, we used the maximum value (e.g., in a range of 2–10% we used 10%). In this way we are sure not to underestimate the measurement uncertainties. In some cases only temperature and critical saturation ratio values were reported, even though the measured variables were temperature and vapor partial pressure. In these cases the unreported vapor partial pressure data were calculated from observed T and S through the given saturation vapor pressure equations. Pressure values given in Torr were converted to Pa.

3. Retrieving the contact parameter

The Classical Nucleation Theory (CNT) allows us to predict the nucleation temperature (or saturation ratio of nucleation onset) as a function of the vapor partial pressure. The heterogeneous CNT can be used either in its full spherical form [35,6,14,27,32] or simplified with the planar approximation (see, for example, Pruppacher and Klett [27].

Our model (based on [19]), which is applicable to heterogeneous vapor-to-liquid nucleation and to deposition mode ice nucleation, includes both the full spherical geometry and the planar approximation. It also uses the accurate heterogeneous Zeldovich factor [33] for the spherical IN case (which reduces correctly in the planar case). We do not include the non-isothermal factor, which is not needed for heterogeneous nucleation, as discussed in Määttänen et al. [20]. For the moment, only single-m deposition mode nucleation is included. The full theory is presented in Appendix B and the planar version in Appendix C. The used values and equations for the thermodynamic data are given in Table A.1 in Appendix A.

The datasets we use have been previously analyzed with the planar theory [12,26]. There are probably two reasons for doing this. First, the used IN are so large (several micrometers in radius) that the planar approximation should not induce large errors, and second, this simple form of the theory can be solved by hand without complicated numerical calculations. In addition, in the studies of Iraci et al. [12] and Phebus et al. [26] the IN particles were deposited on a flat surface, which may participate as a nucleation site. However, for very small particles (radius around or below 100 nm), it might be necessary to use the full theory since the effect of the size of the IN becomes significant [6,1].

3.1. Planar approximation: IN sizes

The applicability of the planar approximation depends on the relative sizes of the forming cluster and the IN: if the IN is much larger than the cluster, the planar approximation can be used. It has been shown by, for example, Määttänen et al. [19] that the IN size starts having a minor effect on the nucleation rate for submicron particles (r_{IN}<1 μm). The effect becomes significant at sizes below (r_{IN}<0.1 μm). We will consider 1 μm as the IN radius below which application of the spherical geometry needs to be tested.

For Trainer et al. [31] the planar approximation is a natural choice, since the experimental data they used had been measured using a planar substrate. The two other studies give very little information on the size distribution of their particles. For Phebus et al. [26] the planar approximation should be applicable, since their particles seemed to be on the larger side, with reported values of volume mean diameter of 8 μm. Same conclusion probably applies to Iraci et al. [12] data, who reported a volume mean diameter of 5 μm for their ATD particles, half of which were smaller than 1.2–1.4 μm. Their clay sample (smectite, [SM]) had 75% of the particles smaller than 2.8 μm in diameter, but they reported the surface area to be dominated by "5–10% of particles with at least one axis $\geqslant$10 μm". It is probable [1,36] that the large particles in these particle samples dominate the nucleation onset and the planar approximation can be applied. Anyhow, we will use both the planar approximation and the accurate spherical version of the heterogeneous CNT on the data of both Iraci et al. [12] and Phebus et al. [26]. However, since we lack information on the size distribution of their IN sample, we will use one particle size only, the choice of which is given below in Table 1. If, as it will be seen, the large particles dominate the nucleation onset, the chosen value for the IN radius does not have an effect on the results. The difference in onset saturation ratio or temperature for IN larger than 1 μm is negligible.

3.2. Method

We propose an alternative method for the estimation of the contact parameter temperature dependence $m(T)$. We test several functional forms in our data inversion. We will only use directly measured values of vapor partial pressure and nucleation onset temperature for the retrieval, and verify the results against the indirectly obtained (calculated) values of critical saturation ratio. We will show how accurately the different functional forms (which we call m-models) can follow the behavior of the data, and we estimate how accurately these limited datasets can reveal the behavior of the contact parameter m as function of temperature. We will apply, for the first time, a well-know data inversion method of Monte Carlo Markov Chains on experimental ice nucleation data, and show its applicability. In future studies we will develop the method further to include other contact parameter distributions.

Recent studies on the shape retrieval [31,12,26] of the contact parameter temperature dependence have assumed an approximation to transform the observed S and T into "measured" m. These data points are then fitted with analytical forms of $m(T)$, such as linear and exponential function of the temperature. Our direct approach is to predict nucleation temperature as a function of pressure assuming a functional shape of $m(T)$ in our nucleation model, and to do the fit in this observational space (temperature and vapor partial pressure) without altering the data. We assume different analytical forms of $m(T)$ (linear, exponential, hyperbolic tangent). Each form depends on a set of parameters $\Theta = \{m_1, m_2, m_3, \ldots\}$ described in Section 3.3. We can thus write the likelihood $\mathcal{L}$ of the model as :

$$2\ln\mathcal{L} = \chi^2(\Theta) = \sum_i^N \frac{\left(T_i^{mod}(\Theta) - T_i^{data}\right)^2}{\sigma_{T,i}^2 + \left(T'\sigma_{p,i}\right)^2} \quad (1)$$

where T_i^{data} and $\sigma_{T,i}$ are the N values and errors on the measured temperatures (in K), $\sigma_{p,i}$ the pressure measurement uncertainties (in Pa), and T' is the derivative of the temperature with respect to pressure (evaluated using the data, in units K Pa^{-1}).

Several approaches are then possible for parameter estimations: likelihood maximization, gridding, or MCMC, for example. The first one can be fast, but it may give a poor estimate of the error bars on the parameters. The second consists in computing on a regular N-dimensional grid of parameters (~20 values per parameter, i.e. 20^N grid points) the values of the likelihood. Then the maximum and the full posterior distribution can be reconstructed. This technique may be slow for a large number of parameters and inefficient if the parameters are strongly correlated. Finally, the MCMC technique allows to sample efficiently the posterior

Table 1
Summary of the used datasets and the parameters (geometry, particle size) used in the nucleation calculations. The symbol ∞ describes either a truly planar substrate or a large IN particle radius, for which the planar approximation can be used.

Experiment	# points	Substrate/IN type	r_{IN}	Plan.	Sphe.	Ref.
Trainer	22	Au/Si	∞	X		Trainer et al. [31]
ATD	11	ATD	2.5 μm 50% < 0.7 μm	X	X	Iraci et al. [12]
SM	11	Smectite	50% < 0.7 μm	X	X	Iraci et al. [12]
JSC	13	JSC Mars-1 Unfractionated	8–300 μm ∞	X		Phebus et al. [26]
	7	JSC Mars-1 Light fraction	<4 μm	X	X	Phebus et al. [26]

distribution and thus find the best model and confidence interval rapidly. We choose the latter method to investigate the shape and parameters describing the contact parameter. This method is commonly used, for example, in cosmology to determine cosmological parameters (age, content of the universe, etc.) from observations (see, e.g., [18,5]). Some atmospheric applications include remote sensing [17] and analyzing aerosol measurement data [28]. The MCMC technique we use is described in Gamerman [8] and MacKay [21].

For each sample (ATD, SM, JSC, Trainer) we run several Markov chains corresponding to the possible behaviors of $m(T)$ with 2, 3, or 4 free parameters. The planar/spherical geometry choice of CNT version to use was made based on the particle size information given in the papers. Information on the datasets, substrates, IN, particle sizes used, and the used geometries in CNT (planar/spherical) are given in Table 1.

3.3. Contact angle parameterization

As explained above, the temperature dependency of the contact parameter is not well defined theoretically, but it has to be deduced from experiments. Depending on the range of temperatures probed by each experiment, the shape of $m(T)$ may appear different. While Iraci et al. [12] and Phebus et al. [26] showed that a linear dependence is enough to explain their data (focused below 200 K), Trainer et al. [31] needed to introduce an exponential behavior to reproduce the plateau at high temperature (above 200 K) and the strong decrease in low temperatures. Both the ascending and asymptotic parts seen in their experiment were well fitted. Yet, such an exponential behavior predicts vanishing contact angle (if not infinitely negative value) at intermediate temperature (around 130K) whereas the contact parameter (a cosine) should range between −1 and 1. We thus propose to test a hyperbolic tangent, which should be easily constrainable within this range, for the temperature dependence of $m(T)$. For each dataset, we reconstruct the best parametric form using the three functionals just described (linear: L, exponential: E, hyperbolic tangent: T), defined as follows (and called from now on the m-models):

$$\mathrm{L}: \; m(T) = m_0 * T + m_1 \tag{2}$$

$$\mathrm{E}: \; m(T) = m_0 - exp(m_1 - m_2 * T) \tag{3}$$

$$\mathrm{T}: \; m(T) = m_2 + ((m_3 - m_2) * tanh(T/m_0)^{m_1}) \tag{4}$$

4. Results

4.1. Results with Trainer et al. [31] data

The Trainer et al. [31] dataset has the largest temperature range. We use the planar approximation only, since the experiments were conducted using a planar substrate.

We remind here that we fit the data in the measured (p, T)-space, as shown in Fig. 2. However, since the final result we are interested in is the $m(T)$, we will illustrate our fits, from now on, only in the (T, m)-space.

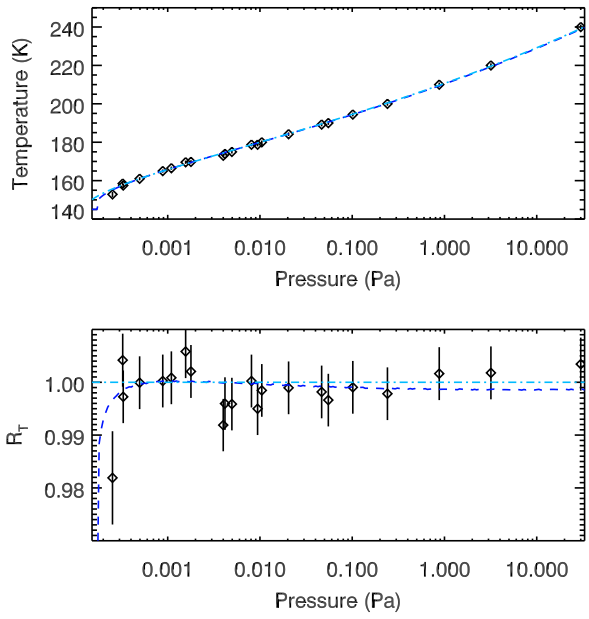

Fig. 2. Best fits to the Trainer data in (p, T)-space for the exponential contact angle $m(T)$ parameterizations. Upper panel: Symbols are the Trainer et al. [31] data points, the turquoise dash-dotted line the Trainer et al. [31] exponential fit and the blue dashed line our exponential fit. Lower panel: The y-axis gives the ratio R_T of the (calculated or measured) nucleation temperature to the nucleation temperature given by the Trainer et al. [31] fit. This means that the turquoise dash-dotted line at 1.00 is the Trainer et al. [31] fit. The data points are the Trainer et al. [31] data points with error bars, and the distance between the dash-dotted line at 1.00 and these points gives the deviation of the fit and the data [31] fit and the data. In this way, the blue dashed line shows simultaneously the deviation of our fit from the data and from the Trainer et al. [31] fit. (For interpretation of the references to color in this figure legend, the reader is referred to the web version of this article.)

As already shown by Trainer et al. [31], the dataset behaves clearly in a non-linear manner: our fits (not shown) confirm that a linear $m(T)$ dependence is not sufficient to describe the dataset. We will try to reproduce the exponential dependence of Trainer et al. [31]. Parameters of the fitted m-models can be found in Table 2.

The left panel of Fig. 3 shows that we reproduce quite well the exponential dependence of m on temperature of Trainer et al [31]. This also validates our approach, since we expect to reproduce well their result when using exactly the same assumptions. The exponential form of $m(T)$ does not quite reach the highest temperature points while following very well the bulk of the dataset in lower temperatures. The highest temperature points come from the gold substrate dataset of Shilling et al. [30], and their error bars (for m) are surprisingly small compared to the other datasets used by Trainer et al. [31]. Our 1σ range (shaded area) does however encompass these points. The exponential m-model has one

Table 2
Results of the linear, exponential, and hyperbolic tangent fits on the four datasets. The functions using the coefficients m_i are given in Eqs. (2)–(4). The symbol – stands for parameter fixed to 0. The values of the previous studies are given in parentheses below the values found in this study. The χ^2_{min}/dof gives the minimum of χ^2 normalized by the degrees of freedom, with the best values shown in bold face type. The line *dof* gives the degrees of freedom of the particular fit.

Sample	ATD			SM			JSC			Trainer		
Model	L	E	T	L	E	T	L	E	T	L	E	T
m_0	0.0045 (0.0046)	0.95	183.07	0.0044 (0.0055)	0.95	147.74	0.0045 (0.0047)	0.999	158.284	0.0041	0.923 (0.94)	144.21
m_1	0.1327 (0.1085)	8.10	7.21	0.1831 (0.0003)	13.89	8.007	0.1387 (0.1184)	5.01	4.244	0.122	10.05 (6005)	3.239
m_2	–	0.065	0.769	–	0.104	−0.471	–	0.044	0.469	–	0.074 (0.065)	−0.698
m_3	–	–	0.995	–		0.942	–	–	0.972	–	–	0.937
χ^2_{min}/dof	0.63 (0.65)	0.639	**0.498**	1.22 (1.26)	0.733	**0.651**	0.262 (0.407)	**0.146**	0.148	1.357	**0.48** (0.52)	0.547
dof	9	8	7	9	8	7	10	9	8	20	19	18

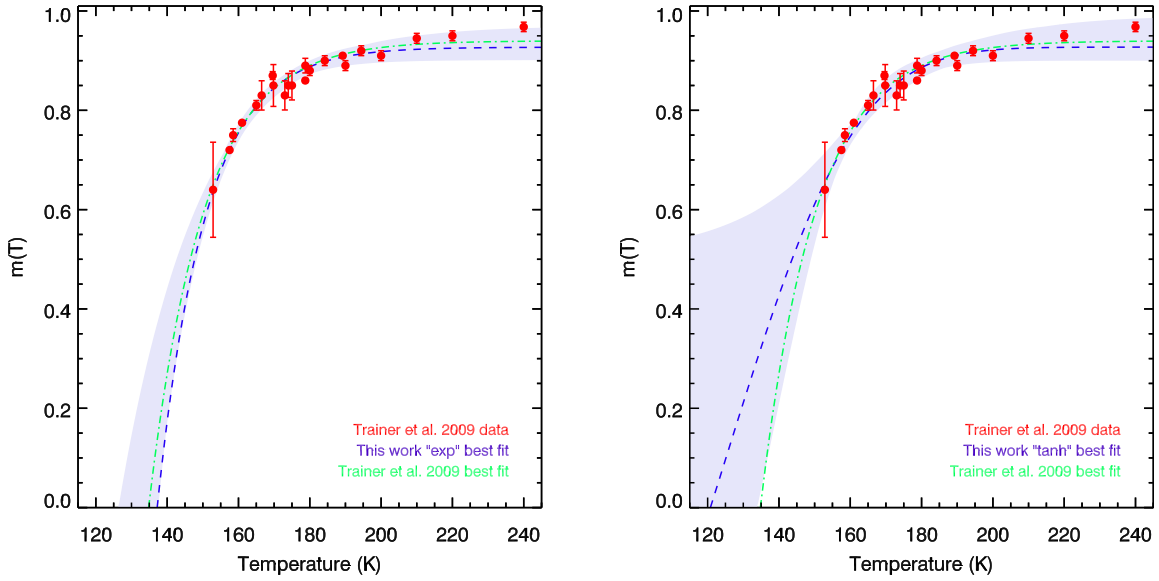

Fig. 3. Best fits to the Trainer data for two parameterizations of the contact angle $m(T)$, exponential on the left and hyperbolic tangent on the right, with confidence intervals (shaded region). Overplotted is the exponential fit from Trainer et al. [31] assuming planar geometry.

practical problem if used in nucleation studies: the $m(T)$ decreases very rapidly towards lower temperatures. In high temperatures the exponential works very nicely since it approaches an asymptotic value below the highest possible value of unity. Such behavior would be helpful also in the lower temperature range, but with the lack of measurements, the low temperature behavior is very difficult to model. We thus propose a new well-behaved functional form of $m(T)$ that captures this asymptotic behavior at both low and high temperatures. What might be a suitable $m(T)$-model for this purpose?

Assuming that m behaves asymptotically (or at least in a less abrupt manner compared to the exponential form) also in low temperatures, we have tested fitting the data using a hyperbolic tangent as the m-model. The hyperbolic tangent has a very similar behavior as the exponential in the higher temperature range, but the decrease in the lower temperature part is more gradual. This m-model can be seen in the right panel of Fig. 3, with the exponential fit of Trainer et al. [31] overplotted. The behavior is overall equally good as with the exponential, but with a less steep decrease below 150 K, as expected. The 1σ limits are of the same range as with the exponential, except in low temperatures, where naturally the behavior is unconstrained in lack of data. However, already with the constraints given by the present dataset, the lower temperature part of the $m(T)$ dependence shows a realistic range of m values even at the steepest decrease, approaching zero around 120 K.

Based on these results on the dataset with the widest temperature range available, we conclude that a linear $m(T)$-model is not sufficient, but a nonlinear model is needed. An exponential or a hyperbolic tangent model are equally good (see Table 2) for fitting the measurement data, with differences only appearing when extrapolating in the lower temperature range where no data points constrain the fit.

4.2. Results with Iraci et al. [12] and Phebus et al. [26] data

Iraci et al. [12] and Phebus et al. [26] fitted their datasets with a linear $m(T)$ behavior and we will begin with the same approach, and then we test the other $m(T)$ dependencies. Furthermore, in general we use the planar geometry, but we also test the spherical geometry when applicable (see Table 1).

The linear m-model result for Iraci et al. [12] ATD sample, assuming planar geometry, is shown in Fig. 4. The behavior is nearly identical when using spherical geometry (not shown), somewhat validating the use of the planar approximation in the data analysis. Our best m-model is close but not identical to that of Iraci et al. [12], nevertheless validating again our approach. However, the possible variation of m-models in the 1σ range is very clear, which means that a unique solution is difficult to find with these data. What should also be noted (as already mentioned by [12] is the rapid increase of $m(T)$ to unity even below 200 K

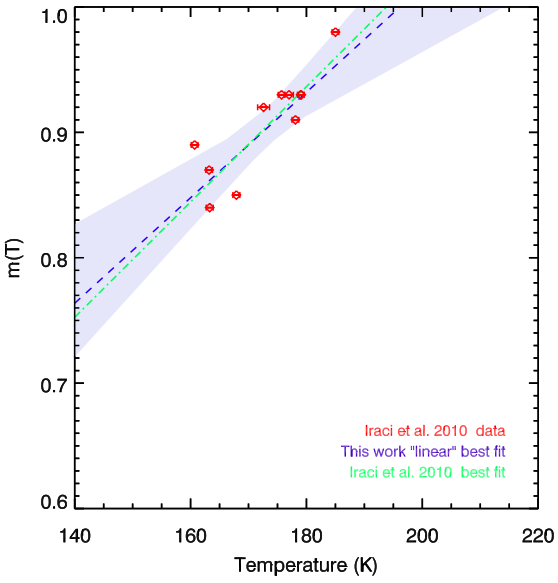

Fig. 4. Best linear m-model (planar only shown) to the ATD data with confidence intervals (shaded region). Overplotted is the Iraci et al. [12] linear fit assuming planar geometry.

predicted by the linear Iraci et al. [12] m-model (which is contrary to measured values, see, e.g., [2]). This raises questions about what value of m to use in practical applications above the temperature range of the measurements.

We obtain similar results for the linear fit of Iraci et al. [12] SM sample (not shown).

In Fig. 5 we show the linear m-model for the unfractionated JSC sample of Phebus et al. [26] (planar geometry only). The same conclusions apply as for Iraci et al. [12]. We do not show here the results of the fit on the measurements of the ground and centrifuged "light fraction" sample, which has very few measurement points, but the conclusions are the same.

In general, the linear m-models applied to these samples show a high degree of degeneracy, particularly for the light fraction sample (not shown) of Phebus et al. [26] that suffers from too few (7) measurement points and a small temperature range. This

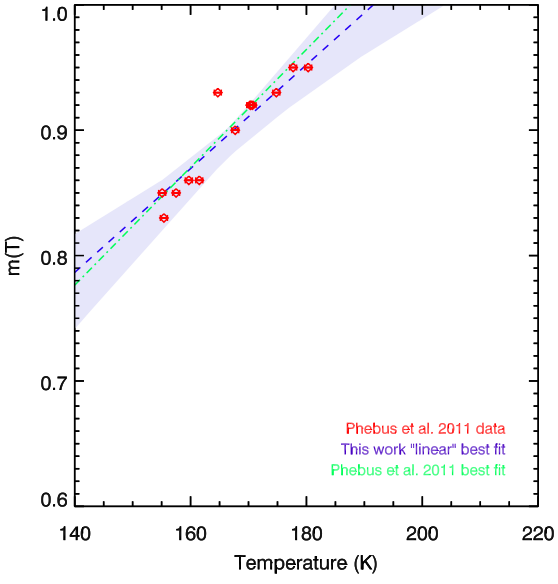

Fig. 5. Best linear m-model (planar only shown) to the JSC data with confidence intervals (shaded region). Overplotted is the Phebus et al. [26] linear fit assuming planar geometry.

implies that more data is required to constrain the slope of the regression. Now the data can be equally well fitted with a large number of linear m-models, as seen in the figures. Table 2 shows that our fits are fully consistent with those published since the χ^2 values are very close. Our results imply that it is very difficult to constrain the $m(T)$ with these datasets, particularly if there are very few data points over a restricted temperature range.

Looking at the overall behavior of the datasets, it looks like the Trainer et al. [31] dataset could be fit with a linear m-model in a narrow temperature range, and only the wider T-range reveals the non-linear behavior. It is very likely that the Iraci et al. [12] and Phebus et al. [26] datasets are unable to reveal the non-linear behavior of $m(T)$ because of the narrow temperature range. We have thus also performed fits with the exponential and hyperbolic tangent m-models to these datasets. We show only results from fits assuming planar approach (no significant differences were found between planar and spherical geometries in these cases, as for the linear ones) for ATD, SM, and JSC samples.

The exponential m-models of Fig. 6 show that indeed, the measurements might be merely revealing the more or less linear part of an exponential behavior. The JSC data can be very well fitted with an exponential behavior of $m(T)$ (see Fig. 6c). Naturally, the lower and higher temperature parts where the models extrapolate the behavior are unconstrained and show fairly large variability, but the behavior in the upper temperature range seems realistic when comparing to the Trainer et al. [31] data points. The fit to the ATD data of Iraci et al. [12] is not improved much from the linear one (see Fig. 6a and b, and Table 2), but the SM fit does seem to improve. The ATD sample (see Fig. 6a) shows large scatter in low temperatures and one very high-m measurement at the highest temperature, making the fitting task very difficult for the exponential m-dependence (the hyperbolic tangent doing a slightly better job, see Table 2).

Following the same deduction as with the Trainer et al. [31] data, we have performed the analysis also with the hyperbolic tangent $m(T)$ dependence, the results of which are shown in the panels of Fig. 7. As might be expected based on the previous results on the Trainer et al. [31] data, the behavior of the m-model is fairly good there where data are available, but shows naturally more uncertainty in the regions of no constraining data points. In the lower temperatures the uncertainty ranges are equally large in all three cases. However, an interesting feature of the hyperbolic tangent models is the behavior at low temperatures. The tail of the best model of the hyperbolic tangent does extrapolate as well as possible the trend set by the data points and clearly different behaviors can be seen between the panels of Fig. 7. Here it should be remembered that the behavior seen in the plotted T, m-space is a consequence of the fit in p, T-space. In the ATD sample (Fig. 7a) the low temperature points show a scatter with some pointing to higher m values at the lowest measured temperatures: the $m(T)$ model emulates this behavior and has a nearly nonexistent slope towards lower temperatures. The SM data (Fig. 7b) has a very steep decrease of m in some of the low temperature data points, extrapolated by the best m-model. The JSC sample (Fig. 7c) is in between these two, constraining well the slope of the $m(T)$ dependence as a consequence of fairly low scatter in the dataset. These results show that a realistic range of $m(T)$ is possible to evaluate with our method, and one of its strengths is its ability to efficiently estimate the range of possible m-model variation. Nevertheless, the low-temperature behavior of $m(T)$ can be fully constrained only with more measurements.

4.3. Result summary

As a summary, the best m-models, measured with the minimum χ^2, acquired for the different data sets are: hyperbolic

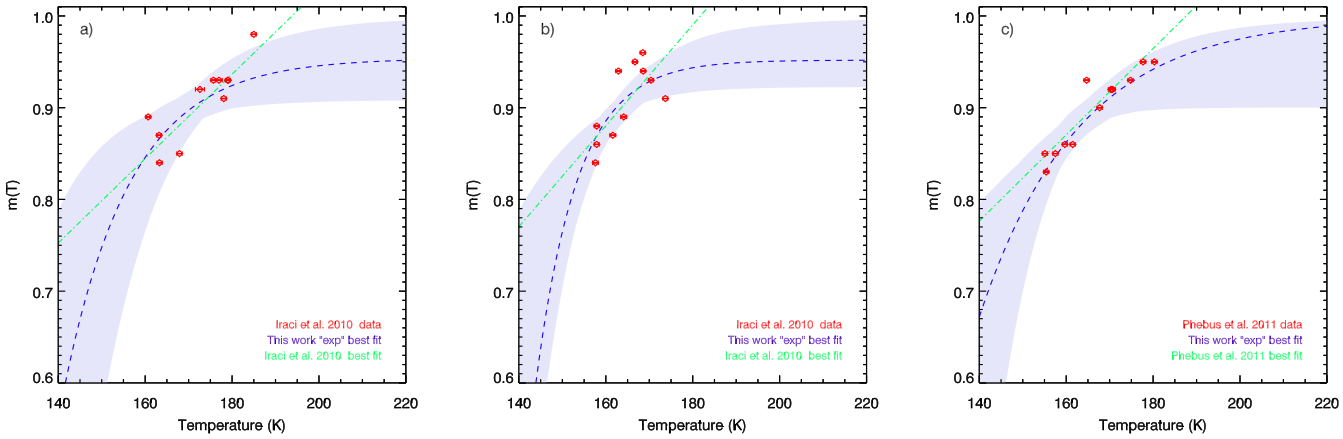

Fig. 6. Best exponential m-models (planar only shown) to the (a) ATD, (b) SM, and (c) JSC data with confidence intervals (shaded region). Overplotted are the linear fits from the respective articles.

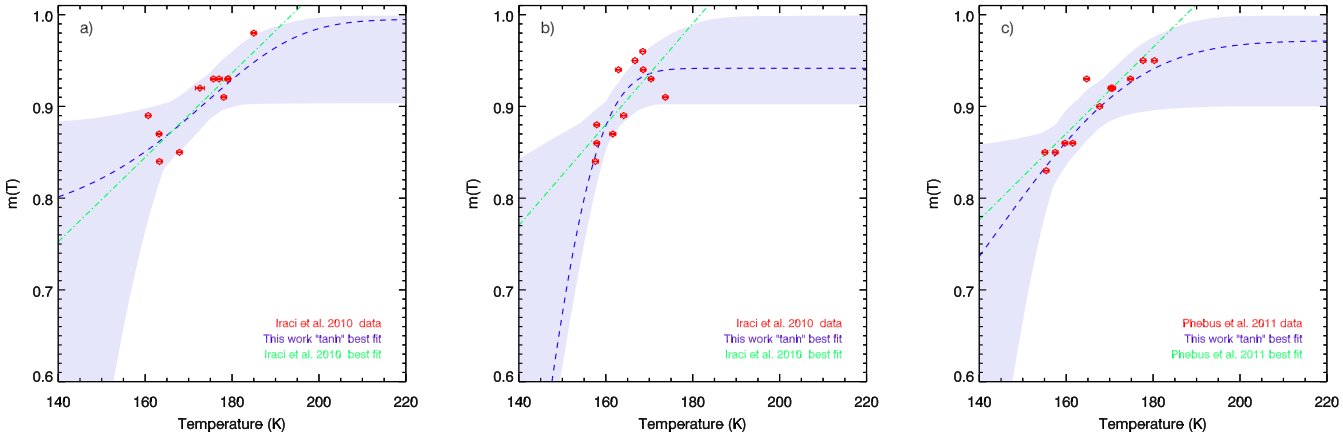

Fig. 7. Best hyperbolic tangent fits of the contact angle $m(T)$ (planar only shown) to the (a) ATD, (b) SM, and (c) JSC data with confidence intervals (shaded region). Overplotted are the linear fits from the respective articles.

tangent for ATD [12], hyperbolic tangent for SM [12], exponential (by a negligible difference to linear and hyperbolic tangent) for JSC [26], and exponential for Trainer [31] data. The hyperbolic tangent fit for Trainer et al. [31] data is only slightly less good than the exponential, because the shape in constrained by the lower limit condition of -1. Relaxing this constraint allows finding an equally good fit as with the exponential. The best m-model found for each dataset, as listed above, is not a function of composition or of IN type, but depends mainly on dataset temperature range. However, these results are based on the datasets and types of IN we analyzed in this work. The m-models depend on the IN type, and an m-model based on experiments of one IN type should not be used to model the $m(T)$ of another type of IN (for example, a dust IN m-model can not describe the behavior of soot as IN, or vice versa).

We would not recommend using the linear m-models unless the temperature range of the application is strictly limited to the temperature range of the original experiments. For the other m-models, the applicability can be estimated based on the application temperature range. If the temperature range is clearly above 170 K, the exponential model describes well enough the behavior of the contact parameter, since it is only the high-temperature end asymptotically approaching unity that is needed in addition to the mid-temperature range. If the temperature range goes below 170 K, the hyperbolic tangent might be the best model to use, but only if the best m-model can be constrained with low-temperature data points.

5. Conclusions

We present a method for analyzing in a robust manner heterogeneous nucleation experiment datasets with the Monte Carlo Markov Chain method coupled to a heterogeneous nucleation model. Our nucleation model uses the Classical Nucleation Theory applicable to heterogeneous vapor-to-liquid nucleation and to deposition mode ice nucleation, and includes both the full spherical geometry and the planar approximation. Using the planar approximation simplifies the calculations required for analyzing the dataset, but it may cause errors with datasets acquired with small IN: this may also force the experimenters to use rather large IN sizes ($r_{IN} > 100$ nm), which might not be relevant in certain cases (high altitudes on Mars or on the Earth). Our method can efficiently analyze the data with the full theory. The method can be used to analyze in a robust manner many kinds of nucleation experiment data, and it can be modified to take into account also other contact parameter distributions than the simplest, single-m description used here. We propose to use the method on any available (at present or in the future) heterogeneous nucleation dataset.

We have applied this method to recent Mars-related datasets on deposition mode ice nucleation of H_2O on different IN and substrates, and we show that it reproduces well the previous results on the temperature dependence of the contact parameter ($m(T)$-model) when exactly the same approximations are used, validating the method. We have also tested the full model in all cases with IN

of possibly submicronic size, but in the datasets used here the difference is not large. This is probably due to the large particles dominating the nucleation efficiency of the samples.

Even though the $m(T)$ dependence is a very important discovery, some of the previous results may be problematic to use in atmospheric applications because of restrained validity ranges. Up until now, there were only a couple of m-models [12,26] with a very limited temperature range applicable to the case of Martian water ice clouds that form with deposition mode ice nucleation onto mineral dust particles. Because of the limited temperature range, these m-models could be used only within this range and the m-values had to be forced to a constant value above and below this range. The upper end of the linear m-model can reach the value of unity if extrapolated outside the temperature range, which is not supported by other experiments [16,2] and would imply perfect wettability and instant activation of the IN for nucleation. It would be very useful to be able to include nucleation into, for example, Martian climate models, but such an m-model is very difficult to use in a cloud modeling application because of these limitations. The Trainer et al. [31] dataset and fit aimed at using a larger temperature range and uncovering the behavior of m in lower temperatures. This study, even if the substrates they used are not comparable to atmospheric IN, showed that the temperature dependence of m can be rather far from linear, and that the asymptotic behavior near unity in high temperatures is a very important feature that needs to be correctly described by an m-model applicable to a large temperature range (in atmospheric modeling for instance). In the present study, in addition to developing the new method for analyzing ice nucleation experiment data, we have tried to combine the two cases explained above. One goal of this work is to provide atmospheric modelers with asymptotically well-behaving m-models that can be applied to the full atmospheric deposition mode ice nucleation temperature range at least on Earth and on Mars, and on other planets, as soon as relevant laboratory experiments are available and analyzed.

The question that stands out is: What is the underlying physical form of the $m(T)$ dependence and are the models we propose here able to represent it accurately? The measured contact parameter accumulates a lot of information on the physical properties of the nucleating surface and the processes occurring, and thus the measured m is always an "effective" contact parameter, integrating the effects of different phenomena (such as active sites and their distribution). The theoretical contact parameter can be defined with the help of surface tensions, which are often described with the help of (temperature and composition dependent) formulae fitted to experimental data and thus may not provide answers either.

We suggest one new (hyperbolic tangent) and test several $m(T)$ dependencies (linear, exponential, hyperbolic tangent). Two of these (exponential and hyperbolic tangent) may be used to avoid unphysical behavior ($m > 1$) in heterogeneous nucleation modeling. However, more measurements are still required to fully constrain these $m(T)$ dependencies. The linear fits published by Iraci et al. [12] and Phebus et al. [26] are probably a result of the narrow temperature range of the experiments, and using a larger temperature range could have uncovered the non-linear behavior of $m(T)$, shown also by our non-linear fits to these data. We do not recommend using linear m-models unless the application is strictly limited to the validity range of the fit, since otherwise unphysical behavior ($m \geqslant 1$) might occur. The exponential m-models behave well at the high and mid-temperature range, but one should be careful when using them at very low temperatures since the m values might decrease very rapidly below the theoretical lowest limit of -1. Exponential m-models should also be obtained for atmospherically relevant IN. The hyperbolic tangent m-models need to be constrained with more low temperature data, but are a promising, physically well-behaving new approach to describe the temperature dependence of the contact parameter.

We show the importance of datasets acquired in a large temperature range for constraining the asymptotic behavior of $m(T)$, and we call for more experiments in a large temperature range, for a range of IN types, well-defined particle sizes or size distributions, and nucleating vapors. In particular, low temperature measurements are needed to be able to extract information on the possible generalized behavior of the contact parameter as a function of temperature. At first, from the point of view of the Earth's atmosphere, it might seem useless to conduct experiments going down to 100–120 K, but the Polar Mesospheric Clouds (PMCs) form at such temperatures. Studying the mechanisms of deposition mode ice nucleation at low temperatures, whatever the applied IN types, are of significance for PMC studies. In addition, on Mars, water ice clouds have been observed at altitudes of about 75 km [34], where the temperatures easily drop down to 100 K. For (global) atmospheric model applications accurate modeling of the formation of these clouds is essential [22,25] and thus nucleation experiments in low temperatures have their importance. Exoplanet atmospheres can have water ice clouds forming as well, enlarging the applicability of nucleation experiment results to the modeling of extrasolar atmospheres that are becoming more and more accessible by observational means in the near future. Vapors other than water are important too: CO_2 ice clouds form on Mars, and Pluto and Triton host ice clouds, not to mention the giant gas planets or exoplanets. For all of the mentioned studies a large range of applicability of any (such as nucleation) parameterization is crucial.

Acknowledgments

We wish to thank L. T. Iraci, B. D. Phebus, and M. G. Trainer for sharing their data and clarifying the many questions we had during this work. We also express our gratitude to H. Vehkamäki for fruitful discussions, and reading and commenting on the manuscript. We are grateful for the two anonymous reviewers for their detailed reviews of the paper.

Appendix A. Thermodynamic data used in the calculations

For the properties of the vapors and solids studied in this paper we have used exactly the same values and equations as the articles we are comparing our work with [31,12,26]. The values, equations and references are listed in Table A.1.

Table A.1
Thermodynamic data used in this work. The constant value of c_1^{het} given is only used in the planar approximation, whereas it is calculated with the given equation (number given) when using the exact model in spherical geometry. For the equation of ice density ρ_i, the temperature should be given in degrees Celsius (marked as $T(^\circ C)$), but for the other equations in degrees Kelvin.

Property	cst. value	Equation	Ref.
c_1^{het} (m^{-2})	10^{19} m^{-2}	Eq. (B.3)	Trainer et al. [31], Pruppacher and Klett [27]
$\sigma_{v,s}$ (J m^{-2})	–	$(141.0-15.0\cdot T)\cdot 10^{-3}$	Hale and Plummer [10]
ρ_i (kg m^{-3})	–	$(0.9167-(T(^\circ C)\cdot 1.75\cdot 10^{-4})-(T(^\circ C)^2\cdot 5\cdot 10^{-7}))\cdot 10^3$	Pruppacher and Klett [27]
$\ln p_{sat}$ (Pa)	–	$(9.550426-(5723.265/T)+3.53068\cdot \ln T-0.00728332\cdot T)$	Murphy and Koop [24]

Appendix B. CNT in spherical geometry

In this Appendix we describe the equations of the Classical Nucleation Theory used in the model. A detailed description of the theory can be found in Volmer [35], Fletcher [6], Keesee [14], Pruppacher and Klett [27] and Vehkamäki [32].

The heterogeneous nucleation rate can be described in the form [32]

$$J_{\text{het}} = \beta_{\text{het}} c_1^{\text{het}} \exp\left(\frac{-\Delta\varphi_{\text{het}}^*}{k_B T}\right) Z_{\text{het}} \tag{B.1}$$

where β_{het} is the growth coefficient, c_1^{het} the concentration of monomers at the IN surface, $\Delta\varphi_{\text{het}}^*$ the formation free energy of the heterogeneous critical cluster, k_B the Boltzmann constant, T the temperature, and Z_{het} the heterogeneous Zeldovich factor.

The growth coefficient β_{het} can be derived using either the direct vapor deposition or the surface diffusion approach, the latter of which dominates and is used here. It is given as the product of the number and the jumping frequency of adsorbed water molecules able to join the cluster:

$$\beta_{\text{het}} = c_1^{\text{het}} 2\pi r_{\text{IN}} \sin\phi \delta \nu_{\text{diff}} \exp\left(\frac{-\Delta\varphi_{\text{diff}}}{k_B T}\right), \tag{B.2}$$

where δ is the average jumping distance of a diffusing molecule, ν_{diff} is the vibration frequency related to the jumps and $\Delta\varphi_{\text{diff}}$ is the surface diffusion activation energy. The term $\sin\phi$ can be calculated from the geometry through $\cos\phi = (r_{IN} - r^* \cos\theta)/d$, where d is the distance between the centers of the (spherical) critical cluster and the condensation nucleus $d^2 = r^{*2} + r_{IN}^2 - 2r^* r_{IN}\cos\theta = r^{*2}(1 + X^2 - 2Xm)$ and $X = r_{\text{IN}}/r^*$.

The surface concentration of monomers is described at steady-state calculated from the incoming and outgoing molecule fluxes [27]

$$c_1^{\text{het}} = \frac{p_v}{(2\pi m_i k_B T)^{1/2} \nu_{\text{des}}} \exp\left(\frac{\Delta\varphi_{\text{des}}}{k_B T}\right) \tag{B.3}$$

where m_i is the mass of a molecule of the condensing vapor, p_v is the partial pressure of the condensing vapor, ν_{des} is the vibration frequency of the adsorbed molecule on the IN surface (usually assumed to be equal to the vibration frequency related to diffusion ν_{diff}), and $\Delta\varphi_{\text{des}}$ the adsorption/desorption energy per molecule.

The free energy of formation of a homogeneous cluster is

$$\Delta\varphi_{\text{hom}} = -\frac{4\pi r^3}{3\upsilon_i} k_B T \ln S + 4\pi r^2 \sigma_{v,s} \tag{B.4}$$

where r is the cluster radius, $\upsilon_i = m_i/\rho_i$ is the molecular volume in the condensed phase calculated with the help of the density of the condensed phase ρ_i, and $\sigma_{v,s}$ is the surface tension between the vapor and the solid phases. The critical free energy of formation of a heterogeneous cluster is

$$\Delta\varphi_{\text{het}}^* = f\Delta\varphi_{\text{hom}}^* = f\frac{16\pi\upsilon_i^2\sigma_{v,s}^3}{3(k_B T \ln S)^2}. \tag{B.5}$$

The geometric factor f in spherical geometry is

$$f = \frac{1}{2}\left(1 + \left(\frac{1 - Xm}{g}\right)^3 + X^3\left[1 - 3\left(\frac{X - m}{g}\right) + \left(\frac{X - m}{g}\right)^3\right] + 3X^2 m\left(\frac{X - m}{g} - 1\right)\right) \tag{B.6}$$

where $g = (1 + X^2 - 2Xm)^{1/2}$. In the case of a planar IN surface ($r_{\text{IN}} \to \infty$), the size parameter $X = r_{\text{IN}}/r^* \to \infty$, and Eq. (B.6) reduces to $f_{\text{planar}} = \frac{1}{4}(2 - 3m + m^3)$.

The radius of the critical cluster

$$r^* = \frac{2\upsilon_i \sigma_{v,s}}{k_B T \ln S} \tag{B.7}$$

is obtained when the derivative of the Gibbs-Thomson equation with respect to radius (B.4) is set to zero.

The heterogeneous Zeldovich factor [33] is given by

$$Z_{\text{het}} = \frac{\upsilon_i}{\pi r^{*2}}\sqrt{\frac{\sigma_{v,s}}{k_B T}}\sqrt{\frac{1}{2 + \frac{(1-mX)[2-4mX-(m^2-3)X^2]}{(1-2mX+X^2)^{3/2}}}} = Z_{\text{hom}}\sqrt{\frac{4}{2 + \frac{(1-mX)[2-4mX-(m^2-3)X^2]}{(1-2mX+X^2)^{3/2}}}}. \tag{B.8}$$

This reduces to the homogeneous Zeldovich factor in the case of non-wettable IN surface ($m = -1$), and if the IN radius approaches zero ($X = 0$).

Appendix C. CNT in planar geometry

This appendix reproduces the equations used in, for example, Trainer et al. [31] for calculating the contact parameters from experiments with the help of nucleation theory. Here we use the same notations as in Appendix B where possible.

The nucleation rate on a planar surface is given by:

$$J = A\exp\left(\frac{-\Delta\varphi_{\text{het}}^*}{k_B T}\right) \tag{C.1}$$

where the formation free energy $\Delta\varphi_{\text{het}}^* = (4/3)(f_{\text{planar}}\pi r^{*2}\sigma_{v,s})$ is the heterogeneous formation free energy that can be calculated when the critical cluster radius at the experimental conditions has been determined from:

$$r^* = \frac{2M_i\sigma_{v,s}}{RT\rho_i \ln S} \tag{C.2}$$

where M_i is the molar mass and R the molar gas constant.

The coefficient A denotes the kinetic pre-factor that includes the effects of the Zeldovich factor, the growth coefficient, and the surface concentration of monomers as described previously. However, the kinetic pre-factor in Trainer et al. [31] is much simpler than the exact spherical formula as described in Appendix B and it is given as:

$$A = \frac{\pi p_v r^{*2} c_1^{\text{het}}}{(2\pi m_i k_B T)^{1/2}}\left(\frac{3\upsilon_i \ln S}{24\pi^2 r^{*3}}\right)^{1/2}. \tag{C.3}$$

Note that Trainer et al. [31] give the value of the molar mass for the variable M_i below this equation in their article (corresponding to our m_i) even if they refer to molecular weight. They use correctly the same variable M_i as the molar mass later on when they calculate the critical cluster radius. The difference between these equations in their article is that one uses k_B and the other R, which determines if m_i or M_i should be used. The geometric factor in planar geometry f_{planar} is:

$$f_{\text{planar}} = \frac{(2+m)(1-m)^2}{4} = \frac{1}{4}(2 - 3m + m^3) \tag{C.4}$$

References

[1] Chen J-P, Hazra A, Levin Z. Parameterizing ice nucleation rates using contact angle and activation energy derived from laboratory data. Atmos Chem Phys 2008;8:7431–49.

[2] Cziczo DJ, Garimella S, Raddatz M, Hoehler K, Schnaiter M, Saathoff H, et al. Ice nucleation by surrogates of Martian mineral dust: what can we learn about Mars without leaving Earth? J Geophys Res 2013;118:1945–54.

[3] DeMott PJ, Cziczo DJ, Prenni AJ, Murphy DM, Kreidenweis SM, Thomson DS, et al. Measurements of the concentration and composition of nuclei for cirrus formation. PNAS 2003;100:14655–60.

[4] DeMott PJ, Sassen K, Poellot MR, Baumgardner D, Rogers DC, Brooks SD, et al. African dust aerosols as atmospheric ice nuclei. Geophys Res Lett 2003;30:1732.

[5] Douspis M, Riazuelo A, Zolnierowski Y, Blanchard A. Cosmological parameter estimation in the quintessence paradigm. Astron Astrophys 2003;405:409–14.
[6] Fletcher NH. Size effect in heterogeneous nucleation. J Chem Phys 1958;29(3):572–6.
[7] Fortin TJ, Drdla K, Iraci LT, Tolbert MA. Ice condensation on sulfuric acid tetrahydrate: implications for polar stratospheric ice clouds. Atmos Chem Phys 2003;3:987–97.
[8] Gamerman D. Markov Chain Monte Carlo: stochastic simulation for Bayesian inference. Chapman Hall; 1997.
[9] Gooding JL. Martian dust particles as condensation nuclei: a preliminary assessment of mineralogical factors. Icarus 1986;66:56–74.
[10] Hale BN, Plummer PLM. Molecular model for ice clusters in a supersaturated vapor. J Chem Phys 1974;61:4012–9.
[11] Hoose C, Möhler O. Heterogeneous ice nucleation on atmospheric aerosols: a review of results from laboratory experiments. Atmos Chem Phys 2012;12(20):9817–54.
[12] Iraci LT, Phebus BD, Stone BM, Colaprete A. Water ice clouds formation on mars is more difficult than presumed: laboratory studies on ice nucleation on surrogate materials. Icarus 2010;210:985–91. doi:10.1016/j.icarus.2010.07.020.
[13] Kahn RA, Martin TZ, Zurek RW. The Martian dust cycle. In: Kieffer HH, Jakosky BM, Snyder CW, Matthews MS, editors. Mars. University of Arizona Press; 1992. p. 1017–53.
[14] Keesee RG. Nucleation and particle formation in the upper atmosphere. J Geophys Res 1989;94(D12):14683–92.
[15] Koehler KA, Kreidenweis SM, Demott PJ, Petters MD, Prenni AJ, Möhler O. Laboratory investigations of the impact of mineral dust aerosol on cold cloud formation. Atmos Chem Phys 2010;10:11955–68.
[16] Ladino LA, Abbatt JPD. Laboratory investigation of Martian water ice cloud formation using dust aerosol stimulants. J Geophys Res 2013;118:14–25.
[17] Laine M, Tamminen J. Aerosol model selection and uncertainty modelling by adaptive MCMC technique. Atmos Chem Phys 2008;8(24):7697–707.
[18] Lewis A, Bridle S. Cosmological parameters from CMB and other data: a Monte Carlo approach. Phys Rev D 2002;66(10):103511.
[19] Määttänen A, Vehkamäki H, Lauri A, Merikallio S, Kauhanen J, Savijärvi H, et al. Nucleation studies in the martian atmosphere. J Geophys Res 2005;110:E02002.
[20] Määttänen A, Vehkamäki H, Lauri A, Napari I, Kulmala M. Two-component heterogeneous nucleation kinetics and an application to Mars. J Chem Phys 2007;127(13):134710.
[21] MacKay DJC. Information theory, inference and learning algorithms. Cambridge University Press; 2003.
[22] Madeleine J-B, Forget F, Millour E, Navarro T, Spiga A. The influence of radiatively active water ice clouds on the Martian climate. Geophys Res Lett 2012;39:23202.
[23] Möhler O, Field PR, Connolly P, Benz S, Saathoff H, Schnaiter M, et al. Efficiency of the deposition mode ice nucleation on mineral dust particles. Atmos Chem Phys 2006;6:3007–21.
[24] Murphy DM, Koop T. Review of the vapour pressures of ice and supercooled water for atmospheric applications. QJR Meteorol Soc 2005;131:1539–65.
[25] Navarro T, Madeleine J-B, Forget F, Spiga A, Millour E, Montmessin F, et al. Global climate modeling of the Martian water cycle with improved microphysics and radiatively active water ice clouds. J Geophys Res 2014;119:1479–95. doi:10.1002/2013JE004550.
[26] Phebus BD, Johnson AV, Mar B, Stone BM, Colaprete A, Iraci LT. Water ice nucleation characteristics of JSC Mars-1 regolith simulant under simulated Martian atmospheric conditions. J Geophys Res 2011;116:4009.
[27] Pruppacher HR, Klett JD. Microphysics of clouds and precipitation. Kluwer Academic Publishers; 1997.
[28] San Martini FM, Dunlea EJ, Grutter M, Onasch TB, Jayne JT, Canagaratna MR, et al. Implementation of a Markov Chain Monte Carlo method to inorganic aerosol modeling of observations from the MCMA-2003 campaign – Part I: Model description and application to the La Merced site. Atmos Chem Phys 2006;6(12):4867–88.
[29] Satheesh SK, Krishna Moorthy K. Radiative effects of natural aerosols: a review. Atmos Environ 2005;39:2089–110.
[30] Shilling JE, Fortin TJ, Tolbert MA. Depositional ice nucleation on crystalline organic and inorganic solids. J Geophys Res 2006;111:D12204. doi:10.1029/2005JD006664.
[31] Trainer MG, Toon OB, Tolbert MA. Measurements of depositional ice nucleation on insoluble substrates at low temperatures: implications for Earth and Mars. J Phys Chem C 2009;113:2036–40.
[32] Vehkamäki H. Classical nucleation theory in multicomponent systems. Berlin Heidelberg: Springer; 2006.
[33] Vehkamäki H, Määttänen A, Lauri A, Napari I, Kulmala M. Technical note: the heterogeneous zeldovich factor. Atmos Chem Phys 2007;7:309–13.
[34] Vincendon M, Pilorget C, Gondet B, Murchie S, Bibring J-P. New near-IR observations of mesospheric CO_2 and H_2O clouds on Mars. J Geophys Res 2011;116:E00J02.
[35] Volmer, M. Kinetik der Phasenbildung. Verlag Von Theodor Steinkopff, Dresden und Leipzig; 1939.
[36] Welti A, Lüönd F, Stetzer O, Lohmann U. Influence of particle size on the ice nucleating ability of mineral dusts. Atmos Chem Phys 2009;9:6705–15.
[37] Wheeler MJ, Bertram AK. Deposition nucleation on mineral dust particles: a case against classical nucleation theory with the assumption of a single contact angle. Atmos Chem Phys 2012;12:1189–201.
[38] Wood SE. Nucleation and growth of CO_2 ice crystals in the Martian atmosphere. Ph.D. thesis. Los Angeles: University of California; 1999.
[39] Young T. An essay on the cohesion of fluids. Philos Trans Roy Soc 1805;95:65–87.